Cortical traveling waves link visual and frontal cortex during working memory-guided behavior.

Canhuang Luo[1,2*], Edward F. Ester[2]

[1]School of Psychology, Shenzhen University, No. 3688, Nanhai Avenue, Shenzhen 518060, China
[2]Department of Psychology and Institute for Neuroscience, University of Nevada, Reno
*Correspondence: luocanhuang@gmail.com

Author Contributions (CRediT Taxonomy):

Conceptualization:	CL
Data Curation:	CL
Formal Analysis:	CL
Funding Acquisition:	EFE
Investigation:	CL, EFE
Methodology:	CL, EFE
Project Administration:	CL, EFE
Resources:	CL, EFE
Software:	CL
Supervision:	EFE
Validation:	CL
Visualization:	CL, EFE
Writing – Original Draft,	CL, EFE
Writing – Review & Editing:	CL, EFE

Funding: Supported by NSF 2050833 (EFE)

Conflicts: Neither author has any competing interests.

Number of Figures: 4

Summary

Working Memory (WM) enables flexible behavior by forming a temporal bridge between recent sensory events and possible actions. Through re-analysis of published human EEG studies, we show that successful WM-guided behaviors are accompanied by bidirectional cortical traveling waves linking sensory cortical areas implicated in WM storage with frontal cortical areas implicated in response selection and production. We identified a feedforward (occipital-to-frontal) theta wave that emerged shortly after a response probe and whose latency predicted intra- and inter-individual differences in response times, and a feedback (frontal-to-occipital) beta wave that emerged after response termination. Importantly, both waveforms were present only around the time of an overt motor response. When participants could select task-relevant WM content prepare but not execute a task-appropriate action, neither waveform was observed. Our observations suggest that cortical traveling waves play an important role in the generation and execution of WM-guided behaviors.

Working memory (WM) is a capacity- and duration-limited system that forms a temporal bridge between fleeting sensory phenomena and possible actions. Classic studies have demonstrated that the contents of WM can be decoded from patterns of fMRI and EEG activity in human early visual cortex (Serences et al., 2009; Harrison & Tong, 2009; LaRocque et al., 2012; Wolff et al., 2017; Rademaker et al., 2019; Kwak & Curtis, 2022), and that the relative quality of stimulus-specific activation patterns measured in visual cortical areas are strong predictors of behavioral WM performance (Ester et al., 2013). These studies support a sensory recruitment model of WM, where WM storage utilizes the same neural machinery responsible for sensory perception. However, WM is fundamentally an action-oriented system: eventually, the contents of WM must be used to produce task-appropriate behaviors. Although recent human and animal studies have documented strong and bidirectional links between systems for WM storage and action (see, e.g., van Ede, 2020, for a recent review), little is known about how sensory brain areas implicated in WM storage communicate with frontal brain areas implicated in the selection and initiation of WM-guided behaviors.

Neural oscillations are known to coordinate communication between distal brain areas (e.g., Fries, 2023). These oscillations often take the form of traveling waves, or spatially coherent oscillations that propagate across the cortex (e.g., Muller et al., 2020). Experimental and theoretical studies suggest that macroscopic traveling waves – i.e., global patterns of activity that extend over several centimeters of the cortical surface – are a key mechanism for guiding the spatial propagation of neural activity and computational processes across the brain (Zhang et al., 2018; Muller et al., 2020). As such, they represent a candidate mechanism for coordinating communication between sensory and frontal areas during WM-guided behavior. Here, we report novel evidence supporting this hypothesis.

Through re-analysis of two published human EEG studies, we show that bidirectional planar traveling waves link visual and frontal electrode sites during WM-guided behavior. In both studies, participants remembered the orientations of two colored bars over a delay and were retrospectively probed to recall the orientation of one bar by adjusting a recall stimulus. Importantly, the physical location of the probed stimulus (i.e., left vs. right visual field) and the hand required for recall (left vs. right) were independently manipulated across trials. This manipulation, coupled with the contralateral organization of human sensorimotor systems allowed us to make trial-wise predictions about the cerebral hemisphere responsible for storing task-relevant WM content and the cerebral hemisphere responsible for producing the task-relevant response. Image-based analyses of EEG data revealed two planar traveling waves around the time of a WM-guided behavior: A feedforward (occipital-to-frontal) theta-band (2-6 Hz) wave that appeared shortly after a response probe and whose peak amplitude predicted intra- and inter-individual differences in response onset, and a later feedback (frontal-to-occipital) beta-band (14-30 Hz) wave that appeared shortly after response termination. Control analyses demonstrated that neither wave could be explained by nuisance factors (e.g., feedforward propagation of visually evoked responses or saccadic eye movements). Importantly, both waveforms required an overt behavioral response: When participants could select and plan a WM-guided behavior but not yet execute it, neither the feedforward theta nor the feedback beta wave was

observed. Collectively, our findings implicate macroscopic cortical traveling waves as an important component in the generation and control of memory-guided actions.

Results

Overview.

To identify cortical traveling waves during WM-guided behaviors, we re-analyzed data from two experiments in two previously published EEG studies (hereafter Experiments 1 and 2; van Ede et al., 2019a; Boettcher et al., 2021, respectively). Both experiments share a similar structure. We first introduce Experiment 1 and later return to Experiment 2.

In Experiment 1, human participants (N = 25) performed a WM recall task that fused components of classic WM and motor control experiments (Figure 1A). Participants remembered the orientations of two colored bars over a short delay. A subsequent change in the color of a central fixation cross (the probe) instructed participants to recall the orientation of the matching bar. Importantly, the tilt of the probe-matching bar told participants which hand should be used for recall, with counterclockwise (clockwise) tilted bars requiring a left hand (right hand) response. Participants recalled the orientation of the probed bar by pressing and holding a button on a computer keyboard with the appropriate response hand. Upon participants' initial button press, a vertically oriented recall stimulus appeared and began to rotate in the selected direction (i.e., clockwise vs. counterclockwise). Participants were instructed to hold the response key down and release it when the orientation of the recall stimulus reached their memory of the probe-matching bar.

A key feature of Experiment 1 (and Experiment 2) is that the physical location (i.e., left vs. right visual field) and vertical tilt (i.e., clockwise vs. counterclockwise) of the probe-matching bar were independently manipulated across trials. For example, a probe-matching stimulus initially presented in the left visual field was equally likely to require a left- vs. right-hand response. This manipulation, coupled with the contralateral organization of sensorimotor systems, allowed us to make trial-wise predictions about the cerebral hemispheres responsible for the storage of task-relevant WM content (i.e., contralateral to the visual hemifield containing the probed bar) and the cerebral hemisphere responsible for producing the appropriate response (i.e., contralateral to the appropriate response hand). For example, we reasoned that participants' report of a left visual field stimulus using the left hand would require coordination between right visual and right motor cortex (Figure 1B).

Measuring Traveling Waves from Human EEG Activity.

To examine whether and how cortical traveling waves contribute to WM-guided behaviors, we applied image-based analyses to EEG recordings obtained while participants performed the memory task summarized in Figure 1A. Since our primary goal was to examine neural dynamics around the commission of a WM-guided behavior, we time-locked our analyses to the probe stimulus that instructed participants which bar to recall (and where the tilt of the to-be-recalled bar instructed participants which hand to respond with). Since traveling waves are thought to depend on horizontal connections between local neural populations (e.g., Ermentrout & Kleinfeld, 2001; Davis et al., 2021; Sato, 2022), we focused our analyses on trials where WM storage and

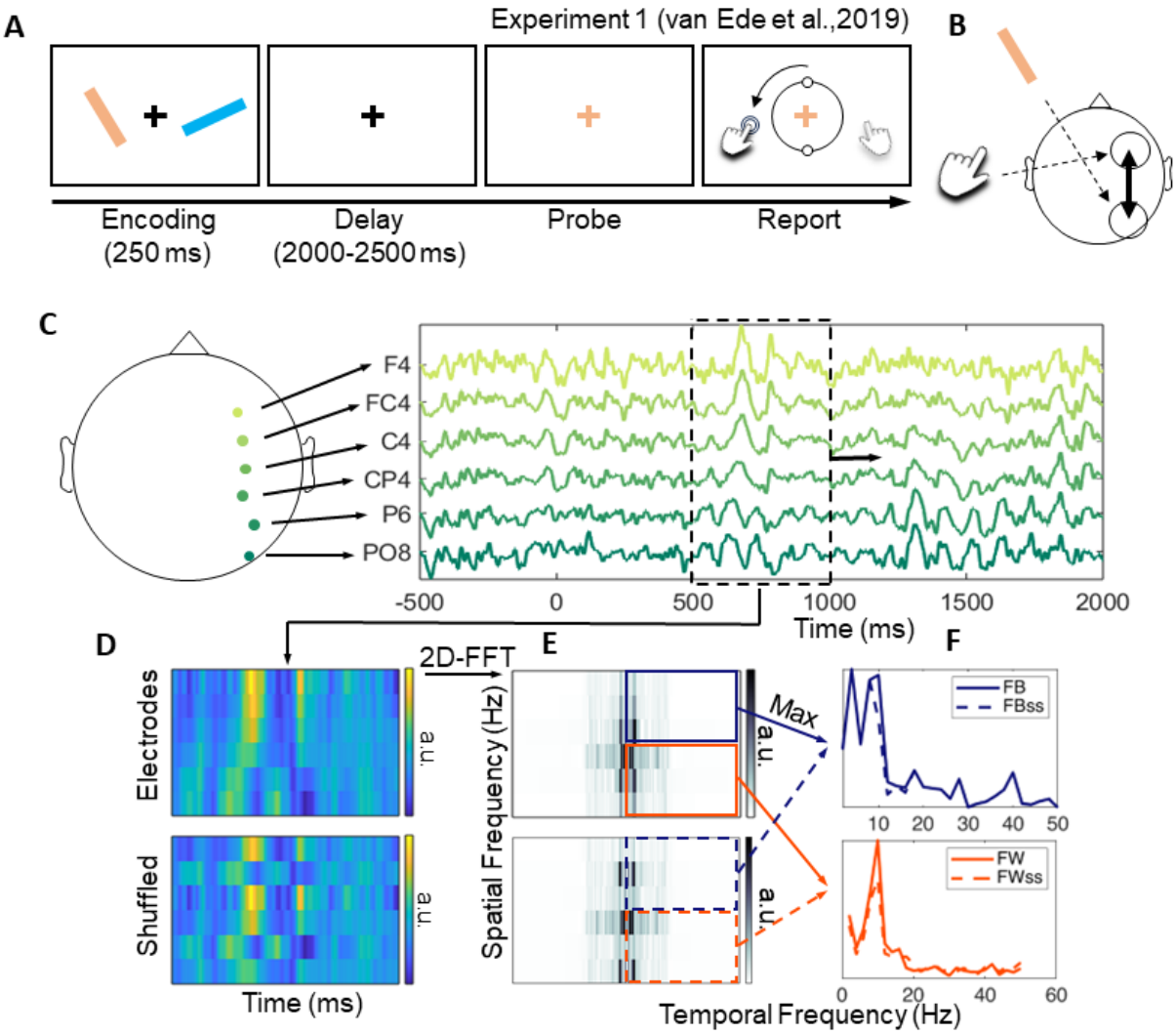

Figure 1. Experiment 1 Schematic and Analytic Approach*. (A) Schematic of the orientation recall task used in Experiment 1 (van Ede et al., 2019a). See text for details. (B) We quantified traveling waves over planar axes contralateral to the location of the retrospectively cued response stimulus (i.e., left vs. right visual hemifield) and the task-relevant response hand (left vs. right). In this example, the storage and report of a left visual field stimulus with the left hand should require communication between right hemisphere visual and frontal areas. (C, D) We defined a planar axis over the task-relevant cerebral hemisphere and created images of EEG activity via a sliding window analysis. (E, F) We used Fourier analysis to extract frequency and phase information from each EEG image and compared forward (occipital-to-frontal; FW) and backward (frontal-to-occipital; FB) phase gradients with surrogate distributions (FWss and FBss) obtained after shuffling electrode labels. See text for additional details.*

WM-guided responses were assumed to depend on the same cerebral hemisphere, e.g., a left (right) visual field stimulus requiring a left (right) hand response.

Following earlier work (Alamia et al., 2023), we defined planar axes linking occipital and frontal electrode sites over each cerebral hemisphere (Figure 1C) and constructed a series of voltage by time images (Figure 1D) by sliding a 500 ms window (50 ms step size) across the EEG signal measured along each axis. We applied a 2-D Fourier transform to each image, yielding a series of spectrographs (Figure 1E) where

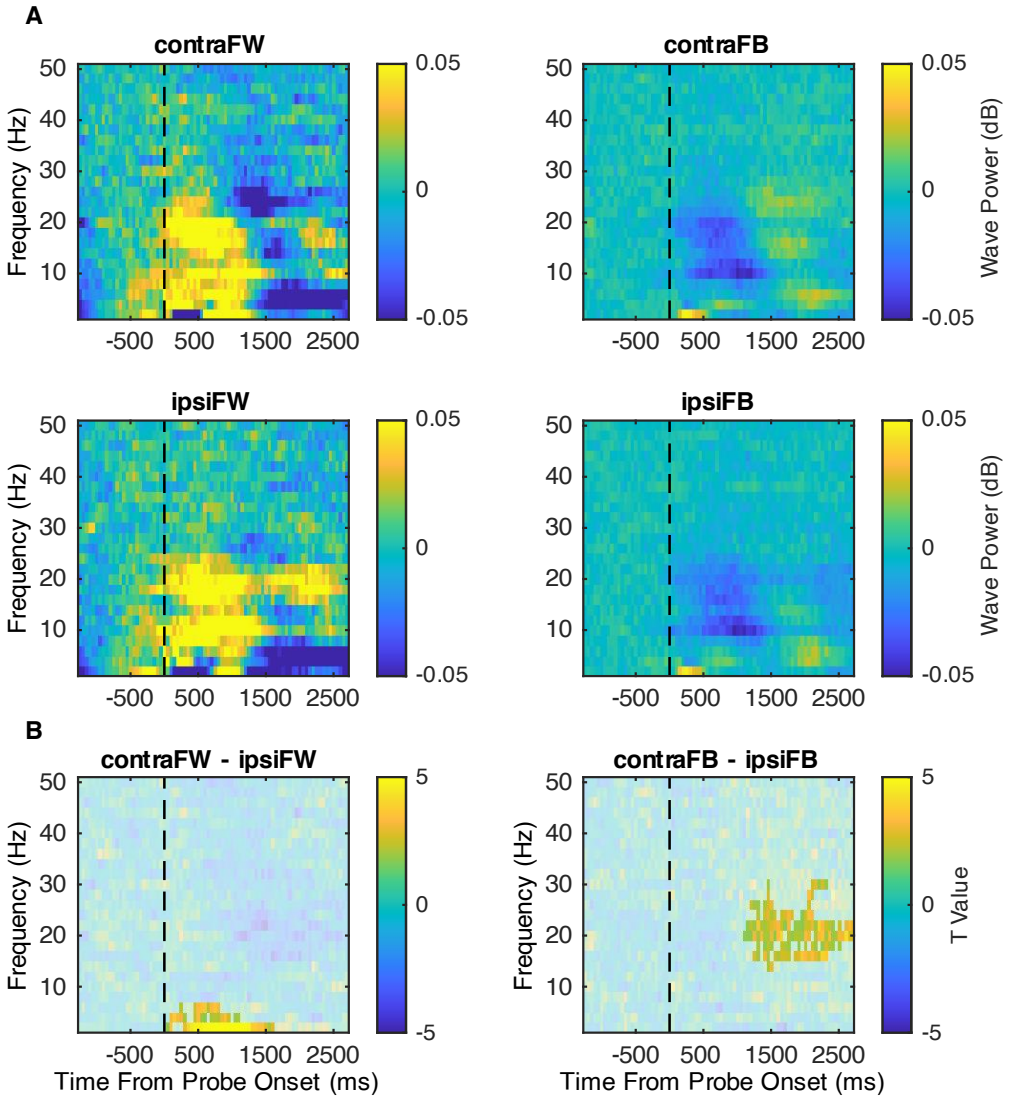

Figure 2. Summary of Probe-Locked Traveling Waves *(A) FW (occipital-to-frontal) and FB (frontal-to-occipital) TW power measured over the task-relevant (contralateral) and task-irrelevant (ipsilateral) cerebral hemispheres. (B) Lateralized TW power, obtained by subtracting ipsilateral from contralateral TW power. The highlighted areas represent significant clusters ($p < 0.05$, cluster-based permutation test).*

the upper and lower quadrants represent energy moving forward (i.e., occipital-to-frontal) and backward (i.e., frontal-to-occipital) along the planar axes, respectively (Figure 1F). We defined frequency-specific forward (FW) and backward (FB) traveling wave power by squaring the absolute value of the complex-valued Fourier coefficients in the top and bottom right quadrants of each spectrograph (note that in this analysis phase information is symmetric around the y-axis). We normalized FW and FB wave power by comparing observed power estimates to estimates from surrogate distributions obtained by re-computing FW and FB wave power after shuffling electrode labels 100 times, expressing total FW and FB wave power as a dB ratio between the

empirical and averaged surrogate data (Figures 1G; 2A). This important step allowed us to compare FW and FB wave power across different times, experimental trials, and participants (Alamia et al., 2023; Luo et al., 2021). Finally, we compared normalized traveling wave power across cerebral hemispheres contralateral vs. ipsilateral to the location of the retrospectively probed WM item and response hand, yielding a lateralized estimate of FW and FB traveling wave power (Figure 2B). Statistical quantification of lateralized traveling wave power estimates (see Methods) revealed a statistically significant FW wave in the theta frequency band (2-6 Hz; Figure 2B left) and a statistically significant FB wave in the beta frequency band (14-30 Hz; Figure 2B right). We therefore extracted, visualized, and analyzed these waveforms separately.

Within-hemisphere feedforward theta and feedback beta waves predict the initiation and cessation of WM-guided behaviors, respectively.

Figure 3A plots normalized FW theta and FW beta wave power time-locked to probe onset (i.e., when participants were instructed to recall the probe-matching bar). FW theta power rose quickly after probe onset and reached a maximum near participants' median response onset time (leading edge of the vertical grey shaded area). This effect was followed by an increase in FB beta power, beginning shortly after the median response offset time (trailing edge of the vertical grey shaded area). We tested these waveforms for links to behavior.

FW theta power reached a maximum near the beginning of participants' responses (Figure 3A), consistent with a role in the generation and implementation of WM-guided behaviors. This interpretation enables three predictions: first, the latency of FW theta power with respect to probe onset should vary with trial-wise variability in participants' response onset times, second, differences in the average latency of FW theta power should robustly predict individual differences in response onset times, and third, the duration of increased FW theta power should vary with response duration (i.e., how long the participants held down the appropriate response button). We tested the first two predictions by quantifying FW theta power after sorting participants' data into fast and slow response onset trials (median split; Figure 3B) and by correlating individual variability in peak theta latency (i.e., the post-probe time at which FW theta power reached its maximum) with participants' median response onset times (Figure 3C). We tested the third prediction by quantifying FW theta power after sorting participants' data into long and short response duration trials (median split; Figure 3D). These analyses confirmed all three of our predictions: FW theta power peaked significantly earlier during fast vs. slow response onset trials ($p < 0.05$, cluster-based permutation test; Figure 3B), individual differences in the peak latency of FW theta power were a strong predictor of participants' median response latencies (robust linear regression: $r^2 = 0.621$, 95% bootstrap CI = 0.0958-0.8893; $p = 1.75e-06$; Figure 3C), and the duration of elevated FW theta power predicted response durations ($p < 0.05$, cluster-based permutation test; Figure 3D). Thus, FW theta waves are strongly linked to intra- and inter-individual differences in the initiation and duration of a WM-guided behavior. We also tested whether peak theta latency predicted intra- or individual

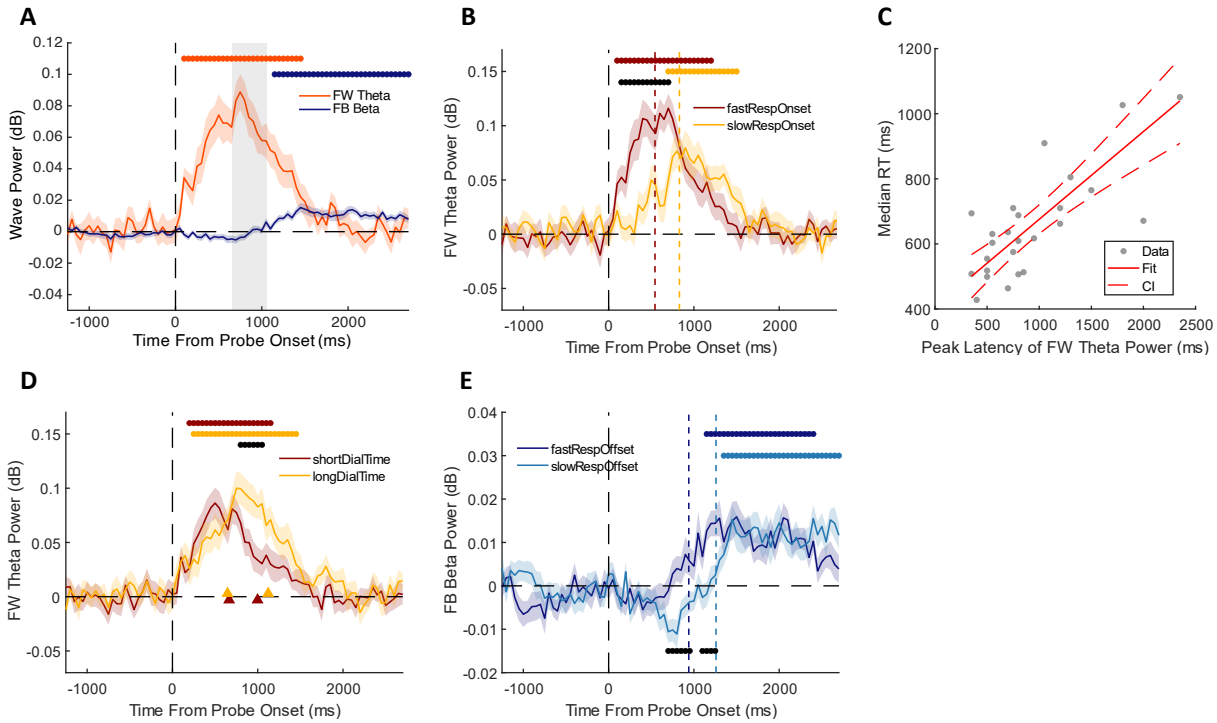

Figure 3. Summary of FW and FB Traveling Waves. *(A) We observed a FW theta wave (2-6 Hz) that emerged shortly after probe onset and that peaked near participants' initial responses (leading edge of grey shaded area), and a later FB beta wave that emerged shortly after participants terminated their response (trailing edge of the gray shaded area). (B) The timing and amplitude of FW theta wave power varied during fast response onset trials (lower 50% of all trials sorted by median response time) and slow response onset trials (upper 50%). The vertical red and yellow dashed lines depict the mean response onset time in the lower and upper 50% of trials, respectively. (C) Individual differences in the peak latency of FW theta wave power predicted participants' median response onset times across all trials. (D) FW theta wave power remained elevated throughout participants responses, lasting longer when participants spent more time rotating the recall stimulus (yellow line) compared to less time rotating the recall stimulus (red line; groups are based on a median split of total rotation time across all trials). The triangles pointing upward denote median response onset and offset corresponding to the long and short response (dial) duration trials. (E) FB beta wave power increased after participants terminated their response, and the latency of FB beta wave power increase was correlated with intra-trial variability in response offset times (i.e., the amount of time that elapsed between probe onset and the termination of participants' responses). Shaded regions in each plot depict ±1 standard error of the mean (SEM); horizontal bars at the top and bottom of each plot depict epochs of statistical significance, with black lines denoting statistical significance between conditions (cluster-based permutation tests; $p < 0.05$; see Methods)*

differences in participants' memory recall (i.e., the mean absolute distance between the correct and reported bar orientation) but found no evidence to support a link (Figure S1).

Unlike FW theta power, FB beta power reached a maximum shortly after participants terminated their response (Figure 3A). In terms of functional relevance, electrophysiological recordings in non-human primates suggest that beta oscillations exercise control over the contents of WM, including the removal of task-irrelevant information (Lundqvist et al., 2018; Miller et al., 2018; Schmidt et al., 2019). We hypothesized that the FB beta wave we observed has a similar function. In the context of Experiment 1, a control mechanism responsible for updating or removing WM contents should only operate when WM-guided behaviors are complete. Therefore, if the FB beta power is related to top-control over WM contents, the latency of this signal

should vary with the termination of WM-guided behaviors. We tested this idea by re-computing FB beta power after sorting participants' trials by response offset, that is, the total elapsed time between probe onset and participants' final key release. Peak FB beta power was delayed by several hundred milliseconds during long-offset trials vs. short-offset trials ($p < 0.05$, cluster-based permutation test; Figure 3E), consistent with a control function for FB beta waves.

Traveling Waves Do Not Cross Cerebral Hemispheres.

Although the precise mechanisms of traveling wave conduction are unknown, both empirical and computational studies suggest a role for short-range horizontal connections between neural populations (e.g., Ermentrout & Kleinfeld, 2001; Davis et al., 2021; Sato, 2022). Conversely, communication between the cerebral hemispheres likely requires signal conduction through deeper callosal or thalamic routes. Under this hypothesis, the within-hemisphere traveling waves summarized in Figures 2 and 3 should be absent during trials where WM storage and response generation rely on different cerebral hemispheres (i.e., a left visual field stimulus requiring a right-hand response). We tested this prediction by computing traveling waves across planar axes linking left (right) occipital electrode sites with right (left) frontal electrode sites. These analyses failed to reveal robust feedforward or feedback waveforms in any frequency band that we analyzed (2-50 Hz; Figure S2).

Traveling Waves are Independent of Visually Evoked Responses and Eye Movements.

In control analyses, we first considered the possibility that FW theta waves were driven by visually evoked responses, i.e., the presentation of the response probe. This is unlikely: since the probe was always presented foveally it should evoke visual responses of equal magnitude across the two cerebral hemispheres, yet FW theta activity was stronger over the cerebral hemisphere contralateral to the task-relevant stimulus and appropriate response hand (Figures 2 and 3A). Nevertheless, to provide a stronger test of the hypothesis that FW theta waves reflect the feedforward propagation of a visually evoked response we re-computed FW theta power after subtracting out EEG activity phase-locked to probe onset (i.e., the visually evoked potential). This step had virtually no effect on FW theta power (or FB beta power; Figure S3); therefore, FW theta waves are unlikely to reflect the feedforward propagation of stimulus-evoked activity.

We also considered the possibility that FW theta and FB beta waves were produced or influenced by saccadic eye movements. Eye position recordings obtained during Experiment 1 indicated that participants' gaze was subtly biased towards the physical location of the task relevant stimulus during recall (reported separately in van Ede et al., 2019b, their Experiment 1). Additionally, large eye movements are known to produce mesoscopic traveling waves in primate visual cortex (e.g., Zanos et al., 2015) and macroscopic traveling waves in scalp EEG recordings (Giannini et al., 2018). Therefore, we tested whether traveling waves were influenced by gaze position by recomputing FW theta and FB beta waves after sorting trials according to whether they contained (a) a horizontal eye movement of any magnitude towards the location of the

probed stimulus, (b) a horizontal eye movement of any magnitude towards the location of the task-irrelevant stimulus, and (c) no detectable horizontal eye movement. Trials were classified into one of these bins if horizontal gaze position exceeded a threshold of 0.057° from fixation at any time from probe onset to response termination. Although FW theta and FB beta waves were noisier (due to splitting the data into three different bins), robust theta and beta peaks were observed in each of these three bins (Figure S4). Thus, FW theta and FB beta waves are unlikely to reflect differences in eye movement patterns across trials.

Traveling Waves Require an Overt Action.

Although FW theta and FW beta waves peaked with response initiation and cessation (respectively; Figure 3A), they need not be linked with action per se. For example, these waves could reflect planning or the generation of a “task set” that describes a plan for upcoming action (e.g., “rotate the recall stimulus by 37 degrees using your right hand”) rather than the execution of that action. We tested this possibility in Experiment 2.

In Experiment 2 (Boettcher et al., 2021; their Experiment 1), human volunteers (N = 26) performed another task that fused elements of WM and motor control. Experiment 2 was identical to Experiment 1 with one exception: a precue display presented prior to the encoding display informed participants which bar would be probed for recall with perfect accuracy (Figure 4A). Therefore, participants could select the task-relevant stimulus and associated response plan (i.e., left vs. right hand) upon presentation of the encoding display, but could not execute their response for several seconds. Indeed, spectral analyses of contemporaneous EEG recordings time-locked to the encoding display revealed decreased alpha lateralization over occipital electrode sites contralateral to the pre-cued stimulus and decreased beta lateralization over frontocentral electrode sites contralateral to the task-relevant response hand, indicating that participants selected the task-relevant stimulus and the task-appropriate response plan (Boettcher et al., 2021; their Figures 2A-C and 3A). However, although participants could (and did) select task-relevant visuomotor information from the encoding display, they were not allowed to act on this information for several seconds. This arrangement provides an ideal scenario to test whether FW theta and FB beta waves reflect the generation of a task set or an action plan. If FW theta and FB beta waves reflect the selection or preparation of a task set, then they should emerge shortly after the appearance of the encoding display and persist through the subsequent delay period. Alternately, if FW theta and FB beta waves are related to overt WM-guided behaviors, then they should only emerge after the appearance of the probe display instructing participants to initiate a response.

Using the same procedures as Experiment 1, we estimated FW theta and FB beta power time-locked to the onset of the encoding display and the onset of the probe display. Analyses time-locked to the probe display revealed a robust FW theta wave that peaked near response initiation and a FB beta wave that peaked after response termination, replicating key findings from Experiment 1 (Figure 4B). However, FW theta and FB beta waves were absent when we time-locked our analyses to the onset of the encoding display (Figure 4C). Importantly, the lack of an effect cannot be explained by

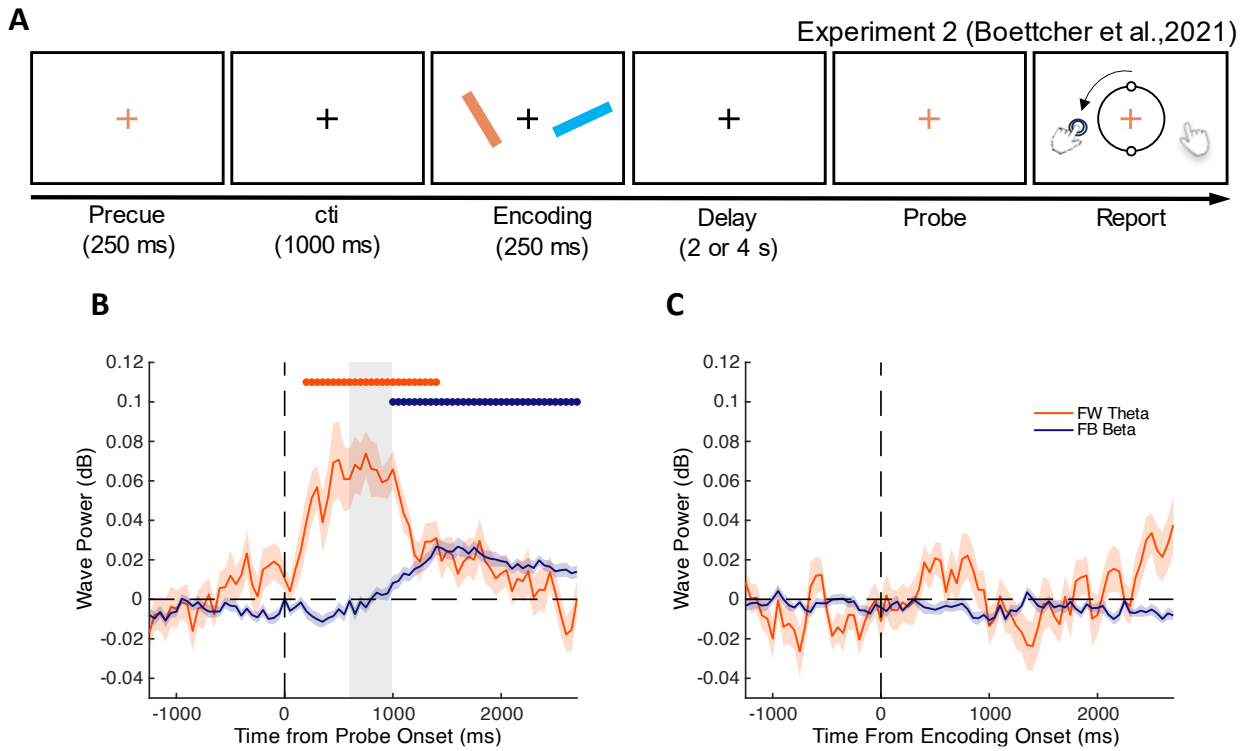

Figure 4. Summary of Experiment 2. *(A) Experiment 2 was like Experiment 1 (Figure 1A), with the exception that the encoding display was preceded by a perfectly informative pre-cue. (B) Analysis of probe-locked EEG data revealed the same FW theta and FB beta were consistent with the results of Experiment 1 (Figure 3A). (C) Analysis of encoding-locked EEG data revealed neither a FW theta wave nor a FB beta wave. Shaded regions in each plot depict the ±1 standard error of the mean.*

participants failing to select the task-relevant bar or task-relevant response plan following the encoding display: as described above, analyses of lateralized EEG signals time-locked to the encoding display revealed clear evidence for visuomotor selection (Boettcher et al., 2021; their Figures 2A-B and 3A). These findings support the view that FW theta and FB beta traveling waves reflect mechanisms related to overt WM-guided behaviors rather than mechanisms related to cognitive control or response preparation.

Discussion

We examined the roles of cortical traveling waves in coordinating the communication of sensory and frontal brain areas during WM-guided behavior through re-analysis of two published EEG studies (van Ede et al., 2019a; Boettcher et al., 2021). Notably, both studies independently manipulated WM storage and response demands in a way that allowed us to make trial-wise predictions about the cerebral hemisphere responsible for WM storage and the cerebral hemisphere responsible for producing task-relevant responses. We identified a feedforward (posterior-to-anterior) theta wave that peaked near the initiation of a WM-guided action and that predicted intra- and inter-individual variability in response times, and a feedback (anterior-to-posterior) beta wave that peaked following the termination of a WM-guided behavior. Neither waveform could be explained by nuisance factors (e.g., feedforward propagation of stimulus-evoked responses or saccadic eye movements), and both waveforms required the generation of an overt motor response: when participants could (and did) select task-relevant WM content and linked motor plans but could not execute an overt movement for several seconds, neither waveform was observed. These observations provide strong and novel evidence that planar cortical traveling waves contribute to the initiation and cessation of WM-guided behaviors, respectively.

Possible Roles for FW Theta and FB Beta Traveling Waves in WM-guided Behaviors.

The precise functional roles of FW theta and FB beta waves cannot be ascertained from the data reported here. Nevertheless, the timing and direction of these waveforms allow for some reasoned speculation. FW theta waves emerged shortly after a response probe, peaked near response initiation, and remained elevated until response termination. We suggest two (non-exclusive) possibilities: first, FW theta waves could reflect a sustained channel that allows visual brain areas responsible for storing WM content to communicate with frontal areas responsible for response planning and execution (i.e., “communication by coherence”; Fries, 2023). Second, FW theta waves could reflect a mechanism that compares stored memory content with external stimuli, e.g., the rotating stimulus participants adjusted to recall orientation. Additional experiments will be needed to test these (and other) possibilities.

FB beta waves emerged shortly after the termination of a WM-guided behavior. Prior research suggests a role for beta oscillations in cognitive and motor control (e.g., Miller et al., 2018; Wessel & Anderson, 2024). Indeed, invasive electrophysiological recordings in non-human primates implicate beta oscillations in top-down control over WM content, such as updating the contents of WM or removing items from WM (Lundqvist et al., 2018; Miller et al., 2018; Schmidt et al., 2019). These findings support the hypothesis that FB beta waves reflect a mechanism that purges WM content to minimize proactive interference. This hypothesis could be tested via experimental manipulations that encourage participants to update or remove the contents of WM mid-trial.

Possible Generators of Cortical Traveling Waves.

Scalp EEG measures cortical oscillations coherent at a spatial scale of centimeters and with geometries that encourage superposition of potentials generated by many local sources (Nunez & Srinivasan, 2006a). Signal distortion caused by volume condition makes it challenging to link EEG potentials with neocortical dynamics. However, theoretical studies suggest that large-scale neocortical electrical fields are sufficient to produce standing and traveling oscillations that can be measured at the scalp (Nunez & Srinivasan, 2006b). In these models, local cell assemblies that drive behavior are embedded within synaptic action fields that reflect short-time changes in the number densities of active excitatory and inhibitory synapses. Recent experimental and theoretical studies suggest that electric fields carry information about WM content (Pinotsis & Miller, 2022) and organize the storage of information across multiple brain areas (Pinotsis & Miller, 2023). We therefore speculate that the directional and frequency-specific traveling waves reported here reflect the operation of large-scale electric fields that shape local cortical activity and information transfer across the neocortex.

Limitations.

The present study focused on traveling waves propagating along planar axes linking posterior and anterior electrode sites. More complicated waveforms may also contribute to WM-guided behaviors. Invasive electrophysiological studies have documented a mixture of planar and rotational (or spiral) waves in monkey prefrontal cortex during WM (Bhattacharya et al., 2022). Additionally, human iEEG studies have documented planar, rotating, and radial traveling waves that predict different aspects of performance on spatial and verbal memory tasks (e.g., Zhang et al., 2018; Mohan et al., 2024; Das et al., 2024). Future work could examine the contributions of complex traveling waveforms in high-density scalp EEG recordings using data-driven methods (e.g., Das et al., 2023).

The present study also focused exclusively on task-aligned traveling waves, i.e., time-locked to probe instructing participants to perform a WM-guided behavior. Spontaneous (i.e., task-independent) traveling waves are also known to contribute to visual task performance. For example, invasive electrophysiological recordings in monkey area MT have revealed the existence of spontaneous traveling waves that predict both the magnitude of target-evoked activity and target detection performance (Davis et al., 2020). Future work could examine the role(s) of spontaneous travelling oscillations in WM-guided behavior and other aspects of WM performance (e.g., encoding or storage).

Broader Implications.

To our knowledge, the present study is the first to characterize cortical traveling waves in a task that independently manipulated cognitive and motor variables, as well as the first to document traveling waves that are contingent on the execution of an overt memory-guided behavior. These observations provide researchers with a new window

to explore putative links between cognitive and motor control, which have heretofore been studied independently (though see Wessel & Anderson, 2024, for a review of studies bucking this trend). Moreover, while the analysis and interpretation of traveling waves from EEG activity can be challenging (see above), it does have some advantages over other approaches. First, iEEG recordings, often characterized as the "gold standard" for understanding human neocortical function, can only be ethically obtained from epileptic patients undergoing neurosurgery. Typically, these surgical interventions are attempted only after years of (unsuccessful) treatment with anticonvulsant medications that influence both neurotransmission and cognition (e.g., Gaitatzis & Sander, 2013). Second, the analysis and interpretation of iEEG data is heavily influenced by electrode placement and electrode size while scalp EEG emphasizes global synaptic field dynamics using standardized electrode placement (i.e., the international 10-10 or 10-20 systems; Nunez & Srinivasan, 2006a). Third, compared to iEEG scalp EEG is universally well-tolerated, including among developmental and geriatric participants and neurological and psychiatric patients. Thus, scalp EEG provides an important vehicle to explore neocortical dynamics – including traveling waves – across healthy and abnormal populations.

Methods

Overview. We reanalyzed data from two published human EEG studies. Experiment 1 used EEG data from van Ede et al. (2019) and eye tracking data from van Ede et al. (2019b); Experiment 2 used EEG data from Boettcher et al. (2021). Detailed methods can be found in each manuscript; for brevity we focus on our own methodological and analytic solutions.

Data Availability: Raw EEG and eye tracking data for each experiment are freely available through repositories maintained by the original authors (see STAR Methods table). We are indebted to the authors for sharing their data with other researchers.

Code Availability: Analyses reported in the current manuscript were carried out with MATLAB (Natick, MA) using open-source toolboxes (EEGLAB, Delorme & Makeig, 2004; FieldTrip, Oostenveld et al., 2011) and custom software. Analytic software sufficient to produce each manuscript figure will be made freely available upon publication of this manuscript.

Participants. 25 human volunteers (14 females) aged 19-36 completed Experiment 1. A different set of 26 human volunteers (19 females) aged 19-25 completed Experiment 2. One participant was excluded from Experiment 2 due to noncompliance with experimenter instructions. Additional details can be found in van Ede et al. (2019a) and Boettcher et al (2021). See also Table 1.

EEG Preprocessing. Raw EEG data were high-pass filtered at 1 Hz and re-referenced to the algebraic mean of external electrodes placed over the left and right mastoids. Re-referenced EEG signals were re-sampled to 300 Hz and epoched from -1500 to +3000 ms around events of interest (e.g., onset of the probe or encoding display).

Estimation and Quantification of Traveling Waves from EEG Data. We estimated and quantified traveling waves using a procedure developed by Almaia and colleagues (Almaia & VanRullen, 2019; Almaia et al., 2023). Trials with unusually fast or slow response onsets (>4 standard deviations from participants' median response time) and trials where participants responded using the wrong hand were excluded from further analyses. This resulted in an average loss of 6.7% of all trials in Experiment 1 and 2.3% of trials from Experiment 2.

We defined planar axes linking frontal and electrode sites over each cerebral hemisphere (10-10 sites O1, PO3, P3, CP3, C3, FC3, and F3 for the left hemisphere and O2, PO4, P4, CP4, C4, FC4, and F4 for the right hemisphere). We generated a series of voltage-by-time images by sliding a 500 ms window (50 ms step size) across each axis (Figure 1D-E), then applied a 2-D Fourier transform to each image. The upper and lower quadrants of the resulting spectrographs depict frequency-specific phase gradients (i.e., traveling waves) moving forward (i.e., occipital-to frontal) and backward (i.e., frontal-to-occipital) along each planar axis, respectively. We compared observed phase gradients with surrogate distributions obtained by re-computing phase gradients

after shuffling electrode labels 100 times. We expressed total wave power as a decibel (dB) ratio between the observed and averaged surrogate distributions, i.e.:

$$W = 10 * \log_{10} \frac{observed}{surrogate}$$

Wave power was estimated for each planar axis on each trial. Power estimates were sorted according to trial variables (i.e., the visual hemifield containing the to-be-recalled stimulus and the required response hand). For within-hemisphere analyses (Figures 2-4), we subtracted wave power over the planar axis ipsilateral to the stimulus' position and response hand from wave power over the planar axis contralateral to the stimulus' position and response hand. Difference waves (i.e., contralateral minus ipsilateral) were then averaged across trials. Statistical significance was estimated using non-parametric cluster-based permutation tests (Maris & Oostenveld, 2007). In brief, we compared empirically estimated difference waves with null distributions of difference waves obtained by randomly flipping the signs of each participant's data 1,000 times. The cluster-based permutation test revealed two significant clusters in the difference waves — theta waves in the 2-6 Hz range and beta waves in the 14-30 Hz range, which were used for further analyses in Figures 2-4.

We used an identical approach to examine the propagation of traveling waves across cerebral hemispheres (Figure S1), with the exception that planar axes were defined using 10-10 electrode sites PO7, PO3, P1, CPz, C2, and FC4 (left occipital to right frontal sites) and PO8, PO4, P2, CPz, C1, and FC3 (right occipital to left frontal sites).

Eye Position Analysis (Experiment 1). During Experiment 1, high-fidelity gaze position estimates were obtained via an SR Research Eyelink 1000 Plus infrared eye tracking system. Binocular recordings were obtained at 1 kHz and later re-sampled to 300 Hz for alignment with contemporaneous EEG recordings. Gaze position data were used to sort experimental trials into three bins: (a) those containing a horizontal eye movement of any magnitude towards the position of the to-be-recalled stimulus, (b) those containing a horizontal eye movement of any magnitude towards the position of the task-irrelevant (i.e., non-recalled) stimulus, and (c) those containing no detectable horizontal eye movement. Trials were assigned to groups (a) or (b) if horizontal gaze position exceeded 0.057° from fixation at any point from probe onset to response termination.

Study	van Ede et al, 2019a	Boettcher et al., 2021
Mean (±1 SD) Trial Count (per participant)	559.8 (±25.07) (25.0732)	312.56 (±9.37) (9.3679)
Participant Information	N = 25 (ages 19-36, 14 females)	N = 26 (ages 18-25, 19 females)
Data link	https://datadryad.org/stash/dataset/doi:10.5061/dryad.sk8rb66	https://zenodo.org/records/4471943

Table 1. Information of datasets used in the current study. The average trial number is the trials remaining for traveling waves analysis.

References

1. Alamia, A., Terral, L., D'ambra, M.R., and VanRullen, R. (2023). Distinct roles of forward and backward alpha-band waves in spatial visual attention. eLife *12*, e85035. 10.7554/eLife.85035.

2. Bhattacharya, S., Brincat, S.L., Lundqvist, M., and Miller, E.K. (2022). Traveling waves in the prefrontal cortex during working memory. PLoS Comput Biol *18*, e1009827. 10.1371/journal.pcbi.1009827.

3. Boettcher, S.E.P., Gresch, D., Nobre, A.C., and Van Ede, F. (2021). Output planning at the input stage in visual working memory. Sci. Adv. *7*, eabe8212. 10.1126/sciadv.abe8212.

4. Das, A., Zabeh, E., Ermentrout, B., and Jacobs, J. (2024). Planar, Spiral, and Concentric Traveling Waves Distinguish Cognitive States in Human Memory (Neuroscience) 10.1101/2024.01.26.577456.

5. Das, A., Zabeh, E., and Jacobs, J. (2022). How can we detect and analyze traveling waves in human brain oscillations? (PsyArXiv) 10.31234/osf.io/jhnpr.

6. Davis, Z.W., Benigno, G.B., Fletterman, C., Desbordes, T., Steward, C., Sejnowski, T.J., H. Reynolds, J., and Muller, L. (2021). Spontaneous traveling waves naturally emerge from horizontal fiber time delays and travel through locally asynchronous-irregular states. Nat Commun *12*, 6057. 10.1038/s41467-021-26175-1.

7. Davis, Z.W., Muller, L., Martinez-Trujillo, J., Sejnowski, T., and Reynolds, J.H. (2020). Spontaneous travelling cortical waves gate perception in behaving primates. Nature *587*, 432–436. 10.1038/s41586-020-2802-y.

8. Ermentrout, G. B., & Kleinfeld, D. (2001). Traveling electrical waves in cortex: insights from phase dynamics and speculation on a computational role. Neuron, 29(1), 33-44.

9. Ester, E.F., Anderson, D.E., Serences, J.T., and Awh, E. (2013). A Neural Measure of Precision in Visual Working Memory. Journal of Cognitive Neuroscience *25*, 754–761. 10.1162/jocn_a_00357.

10. Fries, P. (2023). Rhythmic attentional scanning. Neuron *111*, 954–970. 10.1016/j.neuron.2023.02.015.

11. Gaitatzis, A., & Sander, J. W. (2013). The long-term safety of antiepileptic drugs. CNS drugs, 27, 435-455.

12. Giannini, M., Alexander, D.M., Nikolaev, A.R., and Van Leeuwen, C. (2018). Large-Scale Traveling Waves in EEG Activity Following Eye Movement. Brain Topogr *31*, 608–622. 10.1007/s10548-018-0622-2.

13. Harrison, S.A., and Tong, F. (2009). Decoding reveals the contents of visual working memory in early visual areas. Nature *458*, 632–635. 10.1038/nature07832.

14. Kwak, Y., and Curtis, C.E. (2022). Unveiling the abstract format of mnemonic representations. Neuron *110*, 1822-1828.e5. 10.1016/j.neuron.2022.03.016.

15. LaRocque, J. J., Lewis-Peacock, J. A., Drysdale, A. T., Oberauer, K., & Postle, B. R. (2013). Decoding attended information in short-term memory: an EEG study. Journal of cognitive neuroscience, 25(1), 127-142.

16. Lee, S.-H., Blake, R., and Heeger, D.J. (2005). Traveling waves of activity in primary visual cortex during binocular rivalry. Nat Neurosci *8*, 22–23. 10.1038/nn1365.

17. Lundqvist, M., Herman, P., Warden, M.R., Brincat, S.L., and Miller, E.K. (2018). Gamma and beta bursts during working memory readout suggest roles in its volitional control. Nat Commun *9*, 394. 10.1038/s41467-017-02791-8.

18. Miller, E.K., Lundqvist, M., and Bastos, A.M. (2018). Working Memory 2.0. Neuron *100*, 463–475. 10.1016/j.neuron.2018.09.023.

19. Mohan, U.R., Zhang, H., and Jacobs, J. (2022). The direction and timing of theta and alpha traveling waves modulate human memory processing (Neuroscience) 10.1101/2022.02.07.479466.

20. Mohan, U.R., Zhang, H., and Jacobs, J. (2023). Direct cortical stimulation modulates propagation directions of traveling wave in humans. Brain Stimulation *16*, 132–133. 10.1016/j.brs.2023.01.060.

21. Muller, L., Chavane, F., Reynolds, J., and Sejnowski, T.J. (2018). Cortical travelling waves: mechanisms and computational principles. Nat Rev Neurosci *19*, 255–268. 10.1038/nrn.2018.20.

22. Nunez, P. L., & Srinivasan, R. (2006). Electric fields of the brain: the neurophysics of EEG. Oxford University Press, USA.

23. Nunez, P.L., and Srinivasan, R. (2006). A theoretical basis for standing and traveling brain waves measured with human EEG with implications for an integrated consciousness. Clinical Neurophysiology *117*, 2424–2435. 10.1016/j.clinph.2006.06.754.

24. Pinotsis, D.A., and Miller, E.K. (2023). In vivo ephaptic coupling allows memory network formation. Cerebral Cortex *33*, 9877–9895. 10.1093/cercor/bhad251.

25. Pinotsis, D.A., Fridman, G., and Miller, E.K. (2023). Cytoelectric coupling: Electric fields sculpt neural activity and “tune” the brain’s infrastructure. Progress in Neurobiology *226*, 102465. 10.1016/j.pneurobio.2023.102465.

26. Pinotsis, D.A., and Miller, E.K. (2022). Beyond dimension reduction: Stable electric fields emerge from and allow representational drift. NeuroImage *253*, 119058. 10.1016/j.neuroimage.2022.119058.

27. Rademaker, R.L., Chunharas, C., and Serences, J.T. (2019). Coexisting representations of

sensory and mnemonic information in human visual cortex. Nat Neurosci *22*, 1336–1344. 10.1038/s41593-019-0428-x.

28. Sato, N. (2022). Cortical traveling waves reflect state-dependent hierarchical sequencing of local regions in the human connectome network. Sci Rep *12*, 334. 10.1038/s41598-021-04169-9.

29. Sato, T.K., Nauhaus, I., and Carandini, M. (2012). Traveling Waves in Visual Cortex. Neuron *75*, 218–229. 10.1016/j.neuron.2012.06.029.

30. Schmidt, R., Herrojo Ruiz, M., Kilavik, B.E., Lundqvist, M., Starr, P.A., and Aron, A.R. (2019). Beta Oscillations in Working Memory, Executive Control of Movement and Thought, and Sensorimotor Function. J. Neurosci. *39*, 8231–8238. 10.1523/JNEUROSCI.1163-19.2019.

31. Serences, J.T., Ester, E.F., Vogel, E.K., and Awh, E. (2009). Stimulus-Specific Delay Activity in Human Primary Visual Cortex. Psychol Sci *20*, 207–214. 10.1111/j.1467-9280.2009.02276.x.

32. Van Ede, F., Chekroud, S.R., and Nobre, A.C. (2019). Human gaze tracks attentional focusing in memorized visual space. Nat Hum Behav *3*, 462–470. 10.1038/s41562-019-0549-y.

33. Van Ede, F., Chekroud, S.R., Stokes, M.G., and Nobre, A.C. (2019). Concurrent visual and motor selection during visual working memory guided action. Nat Neurosci *22*, 477–483. 10.1038/s41593-018-0335-6.

34. Wessel, J.R., and Anderson, M.C. (2024). Neural mechanisms of domain-general inhibitory control. Trends in Cognitive Sciences *28*, 124–143. 10.1016/j.tics.2023.09.008.

35. Wolff, M.J., Jochim, J., Akyürek, E.G., and Stokes, M.G. (2017). Dynamic hidden states underlying working-memory-guided behavior. Nat Neurosci *20*, 864–871. 10.1038/nn.4546.

36. Zanos, T.P., Mineault, P.J., Nasiotis, K.T., Guitton, D., and Pack, C.C. (2015). A Sensorimotor Role for Traveling Waves in Primate Visual Cortex. Neuron *85*, 615–627. 10.1016/j.neuron.2014.12.043.

37. Zhang, H., Watrous, A.J., Patel, A., and Jacobs, J. (2018). Theta and Alpha Oscillations Are Traveling Waves in the Human Neocortex. Neuron *98*, 1269-1281.e4. 10.1016/j.neuron.2018.05.019.